International Journal of Humanoid Robotics

External Force Observer for Small and Medium-sized Humanoid Robots*

Louis Hawley, Rémy Rahem and Wael Suleiman
Electrical and Computer Engineering Department, Faculty of Engineering, University of Sherbrooke, Canada
{Louis.Hawley, Remy.Rahem, Wael.Suleiman}@USherbrooke.ca

Received Day Month Year
Revised Day Month Year
Accepted Day Month Year

Corresponding Author (Wael Suleiman)

External force observer for humanoid robots has been widely studied in the literature. However, most of the proposed approaches generally rely on information from six-axis force/torque sensors, which the small or medium-sized humanoid robots usually do not have. As a result, those approaches cannot be applied to this category of humanoid robots, which is widely used nowadays in education or research.

In this paper, we propose a Kalman filter-based observer to estimate the three components of an external force applied in any direction and at an arbitrary point of the robot's structure. The observer is simple to implement and can easily run in real time using the embedded processor of a small or medium-sized humanoid robot, such as Nao or Darwin-OP. Moreover, the observer does not require any changes to the robot's hardware, as it only uses measurements from the available force-sensing resistors (FSR) inserted under the feet of the humanoid robot and from the robot's inertial measurement unit (IMU).

The proposed observer was extensively validated on a Nao humanoid robot in both cases of standing still or walking while an external force was applied to the robot. In the conducted experiments, the observer successfully estimated the external force within a reasonable margin of error. Moreover, the experimental data and the MATLAB and C++/ROS implementations of the proposed observer are available as an open source package.[a]

Keywords: Force observer; External force; Small humanoid robots; Kalman filter; FSR; IMU

1. Introduction

Having a biped structure and articulated arms makes humanoid robots ideal candidates to perform a variety of manipulation and transportation tasks. However,

*A preliminary version of this paper has been presented at the 2018 IEEE/RSJ International Conference on Intelligent Robots and Systems (IROS 2018) and published in Hawley et al (2018) [1].
[a]https://goo.gl/VkhejY

the manipulation or transportation of an object may create instability for the humanoid robot if no measurements are taken to consider the added force, which is generated by the transported object, and adjust the walking gait. Moreover, physical interaction with a human, such as collaboratively transporting an object, also generates interaction forces that should be taken into account to prevent instability issues. In those cases, it is primordial to accurately estimate the forces acting on the humanoid robot.

As an example, the transportation of a heavy object on a rolling cart, as depicted in [2, 3], can be greatly improved if the external force generated by the cart and the transported object can be accurately measured or estimated. Moreover, for a cooperative transportation task of an object with two humanoid robots [4, 5] or with a humanoid robot and a human [6], it is crucial to measure the force exchanged through the transported object in order to maintain the equilibrium of the whole system.

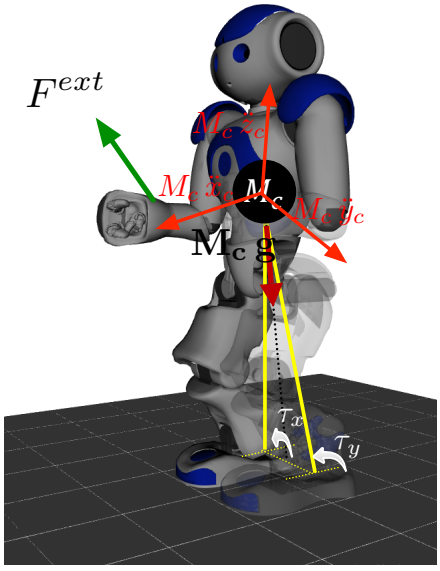

Fig. 1. An external force applied to a Nao robot

In this paper, we consider the case of an external force applied to the humanoid robot as illustrated in Fig. 1.

1.1. *Relevant Works*

There are multiple approaches to estimate external forces exerted on a humanoid robot. These approaches can be roughly separated into three main categories :

sensor-based approaches, model-based approaches and alternative methods such as machine learning-based methods. Each category is summarized with some examples in the following sub-sections.

1.1.1. *Sensor-based Approach*

The sensor-based approach directly measures the external force applied to a humanoid robot by using the robot's sensors. Such a method was used in [7,8], where a pushing manipulation task was performed by a HRP-2 robot. In that case, the external force applied to the humanoid robot can be directly measured at all time using the six-axis Force/Torque (F/T) sensors embedded in the robot's wrists. Then, by considering the external force, the authors were able to apply the required compensation on the torso position to ensure the stability of the robot while pushing the object.

A similar approach has also been proposed by the same authors to enable a humanoid robot to lift and transport a heavy object [9]. The sensor-based approach obviously provides great performance, since the force can be accurately measured at all times. However, F/T sensors are not available on all robots and it would be difficult to integrate them on smaller and cheaper robots due to the size and cost of such sensors.

1.1.2. *Model-based Approach*

We define model-based approach as the methods that estimate the external force acting on a humanoid robot by using a dynamic model of the robot and its actual state vector. For instance, the method presented in [10], where the magnitude of an external force is estimated using a disturbance observer. The observer uses measurements from the robot's IMU and from F/T sensors located in the ankles to estimate the magnitude of a strong force, such as a kick to the robot's chest. In order to estimate the disturbance, the authors used a simplified dynamic model of the humanoid where the acceleration of its Center of Mass (CoM) is a function of the forces applied to the robot, which are: the gravity, the floor reaction force and the unknown external forces. Since the acceleration of the robot's CoM is known using IMU measurements and the floor reaction force can be directly measured with the F/T sensors, their results show that a strong impact force can be estimated somewhat accurately using that model. Another interesting method that can also estimate the external moment is proposed in [11]. That method relies on a model-based estimator to fuse the data of the robot's sensors (F/T sensors and IMU) and the whole body dynamics. An advantage of this approach over the previously presented sensor-based approach is that the external force/moment do not have to be applied at a particular point in order to be estimated. However, these methods still require F/T sensors.

A similar approach has been presented in [12] to enable a humanoid robot to walk

on low friction floor. Using the linear inverted pendulum (LIP) model to represent the humanoid robot, the authors predicted the ground reaction force and compared it with the measurements from F/T sensors in the ankles of a HRP-2 robot. The difference between the two values was then attributed to a slip force that can be easily derived. Although a slip force is also a strong force of short duration, which is very different from the force encountered in interaction tasks between several robots or a robot and a human, these works are interesting as they show that it is possible to get a good estimation of an external force by only using a limited number of sensors and a simple dynamic model of the robot. Such an approach would be interesting for medium-sized humanoid, such as Nao humanoid robot, as they usually have a small number of sensors and limited computational power. Nao [13] is a medium-sized humanoid robot manufactured by SoftBank Robotics.

In [14], the Nao robot's limbs are modeled as kinematic chains attached to the pelvis of the robot, and a relation between a force acting on each link of the robot and the joint torques is established, a method commonly used for serial manipulators. Since Nao's joints do not possess torque sensors nor do they provide a torque estimation, the authors had to define an actuator model to estimate the motor torque from the steady-state error. Then the problem is transformed into isolating the torque caused by gravity to obtain the portion of the torque that is the result of the external force. Although this approach can be quite powerful as the magnitude of the force along with the contact point can be found, there are multiple limitations in the proposed implementation. For instance, it uses the motors steady-state error to estimate the actuator torque. That means the proposed algorithm is only able to estimate big external forces.

Rotella et al. [15] presented some formulations to estimate the CoM position of a robot and to correct inaccuracies in the robot links model. With regard to our work, the most interesting contribution is an external wrench estimator that uses a linear and angular momentum model of the robot instead of the simplified LIP model dynamic. However, the approach is limited to humanoids equipped with F/T sensors at the end-effectors.

Another model-based method to estimate the magnitude of an external force applied to a humanoid robot is presented in [16]. Its main advantage is that it does not require using F/T sensors but instead it uses measurements from the robot's force-sensing resistors (FSR) sensors. The approach has been successfully validated on a Nao robot and pointed out that an external force applied to the robot can be efficiently estimated with an acceptable precision. However, the main limitation of that method is that the formulations are only valid for an external force applied in the horizontal plane. That limitation has been addressed in [1] to handle an external force applied in any direction.

1.1.3. *Alternative Methods*

Machine learning based approaches have also proven to be useful in estimating an external force applied to medium-sized/small humanoid robots.

In [17], perturbations transmitted to a Nao robot are detected by comparing the actual sensor measurements with the predicted ones obtained with a probabilistic model. Using this method, the authors were able to successfully detect and provide an estimation of the perturbation magnitude. However, the external force that generates the perturbation has never been quantified since the algorithm can either provide the difference between the sensors (IMU and FSR) measurements and the predicted values or the difference between the expected footstep length and the equivalent footstep length. Although it is certainly possible to estimate the force from these results, such analysis has not been conducted.

In [18], the authors present a complimentary filter formulation to estimate the CoM of a robot or human. The proposed filter uses a spectral approach to analyze the different methods used to estimate the position of the CoM (i.e. motion capture, contact forces and moments). Then the authors propose to fuse the data by optimally using each sensor. Obviously, this approach requires a diverse set of sensors to span the whole frequency range, a condition that is often not satisfied in the case of small humanoid robots.

2. Contribution

The main contribution of this paper is the design of a model-based observer that is able to estimate the three components of an external force applied to a humanoid robot. The force is projected onto the CoM frame and therefore can be directly used, for instance, in a pattern generator. The observer design and implementation architecture are given in Section 5.

This observer was also validated on a Nao humanoid robot through several experimental scenarios. The results of these experiments are analyzed in Section 6.

3. ZMP with an external force

To study the impact of an external force on the Zero-Moment Point (ZMP) formulation [19], we consider the two following cases:

3.1. *An External Force Directly Applied to the Robot's CoM*

This case study is illustrated in Fig. 2. The ZMP can be found by considering the forces acting on the simplified LIP model, which are the gravity, the inertial force and the external force.

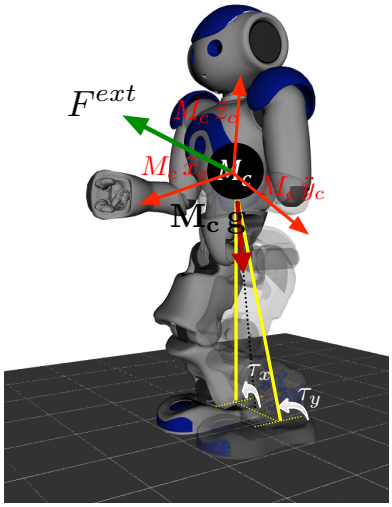

Fig. 2. An external external force applied to the CoM of a Nao robot

Let the ZMP on the horizontal ground be given by the following vector[b]:

$$\boldsymbol{p} = \begin{bmatrix} p_x \\ p_y \end{bmatrix} \tag{1}$$

where p_x and p_y are respectively the projections of the ZMP on the x and y axis.

To compute $\boldsymbol{p}$, one can use the following formula:

$$\boldsymbol{p} = \boldsymbol{N}\ \frac{\boldsymbol{n} \times \boldsymbol{\tau}^o}{(\boldsymbol{f}^o | \boldsymbol{n})} \tag{2}$$

where the operators $\times$ and $(.|.)$ design respectively the cross and scalar products, and

- $\boldsymbol{N}$ is a constant matrix

$$\boldsymbol{N} = \begin{bmatrix} 1 & 0 & 0 \\ 0 & 1 & 0 \end{bmatrix} \tag{3}$$

- the vector $\boldsymbol{n}$ is the normal vector on the horizontal ground $\left(\boldsymbol{n} = \begin{bmatrix} 0 & 0 & 1 \end{bmatrix}^T\right)$.
- The vector $\boldsymbol{f}^o$ is the result of the gravity, inertial and external force:

$$\boldsymbol{f}^o = M_c \boldsymbol{g} - M_c\, \ddot{\boldsymbol{X}}_c + \boldsymbol{F}^{ext} \tag{4}$$

where $\boldsymbol{g}$ denotes the gravity acceleration ($\boldsymbol{g} = -g\boldsymbol{n}$), M_c is the total mass of the humanoid robot, and $\ddot{\boldsymbol{X}}_c = [\ddot{x}_c\ \ddot{y}_c\ \ddot{z}_c]^T$ is the acceleration of the CoM. $\boldsymbol{F}^{ext} = [F_x\ F_y\ F_z]^T$ is the external force applied to the humanoid robot.

[b]As a general rule, ***bold*** parameters are vectors or matrices

The normal force is given by the following expression:

$$(\boldsymbol{f}^o|\boldsymbol{n}) = f_n^o = -M_c\, g - M_c\, \ddot{z}_c + F_z \tag{5}$$

- $\boldsymbol{\tau}^o$ denotes the moment of the external force and the moment of the force $\boldsymbol{f}^o$ about the origin of the fixed world frame. It is given by the following expression:

$$\boldsymbol{\tau}^o = \boldsymbol{X}_c \times \boldsymbol{f}^o \tag{6}$$

where $\boldsymbol{X}_c = \begin{bmatrix} x_c & y_c & z_c \end{bmatrix}^T$ is the Cartesian position of the CoM.

Thus, we obtain:

$$\boldsymbol{p} = \begin{bmatrix} p_x \\ p_y \end{bmatrix} = \begin{bmatrix} x_c + \frac{M_c\, z_c}{f_n^o}\, \ddot{x}_c - \frac{z_c}{f_n^o}\, F_x \\ y_c + \frac{M_c\, z_c}{f_n^o}\, \ddot{y}_c - \frac{z_c}{f_n^o}\, F_y \end{bmatrix} \tag{7}$$

3.2. *An External Force Applied to a Point of the Robot*

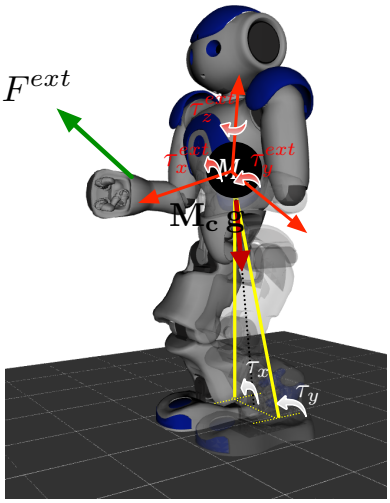

Fig. 3. An external moment is applied to the CoM of the LIP model as a result of an external force applied to a point of Nao robot. The accelerations are omitted for clarity

An external force applied to a point of the robot structure generates an additional external moment applied to the CoM of the LIP model as shown in Fig. 3. For instance, this force could be the result of the robot pushing, pulling or lifting an object or interacting/collaborating with a human.

Similarly to the previous case, the resultant force applied to the LIP model is:

$$\boldsymbol{f}^o = M_c \boldsymbol{g} - M_c \, \ddot{\boldsymbol{X}}_c + \boldsymbol{F}^{ext} \tag{8}$$

However, the moment $\boldsymbol{\tau}^o$ in this case becomes:

$$\boldsymbol{\tau}^o = \boldsymbol{X}_c \times \boldsymbol{f}^o + \boldsymbol{\tau}^{ext} \tag{9}$$

By applying the formula in (2), we obtain:

$$\begin{aligned} \boldsymbol{p} &= \begin{bmatrix} p_x \\ \\ p_y \end{bmatrix} \\ &= \begin{bmatrix} x_c + \frac{M_c \, z_c}{f_n^o} \, \ddot{x}_c - \frac{z_c}{f_n^o} \, F_x - \frac{1}{f_n^o} \, \tau_y^{ext} \\ \\ y_c + \frac{M_c \, z_c}{f_n^o} \, \ddot{y}_c - \frac{z_c}{f_n^o} \, F_y + \frac{1}{f_n^o} \, \tau_x^{ext} \end{bmatrix} \\ &= \begin{bmatrix} x_c + \frac{M_c \, z_c}{f_n^o} \, \ddot{x}_c - \frac{z_c}{f_n^o} \left(F_x + \frac{\tau_y^{ext}}{z_c} \right) \\ \\ y_c + \frac{M_c \, z_c}{f_n^o} \, \ddot{y}_c - \frac{z_c}{f_n^o} \left(F_y - \frac{\tau_x^{ext}}{z_c} \right) \end{bmatrix} \end{aligned} \tag{10}$$

It is clear from (10) that, without additional sensors such as a six-axis F/T sensor, the components of an external force and moment cannot be estimated. However, by defining the following virtual force:

$$\begin{aligned} \hat{\boldsymbol{F}}^{ext} &= \begin{bmatrix} \hat{F}_x \\ \hat{F}_y \\ \hat{F}_z \end{bmatrix} \\ &\triangleq \begin{bmatrix} F_x + \frac{\tau_y^{ext}}{z_c} \\ F_y - \frac{\tau_x^{ext}}{z_c} \\ F_z \end{bmatrix} \end{aligned} \tag{11}$$

One can figure out that, from the ZMP point of view, the impact of an external force $\boldsymbol{F}^{ext}$ applied to a point of the robot is the same as a virtual force $\hat{\boldsymbol{F}}^{ext}$ applied directly to the CoM of the LIP model. Therefore, we only consider the latter case in the sequel of the paper.

4. Measurements

Using the robot's available sensors (FSR, IMU and joint encoders), the ground reaction force, the ZMP, and the acceleration and position of the CoM can all be estimated. Those variables will play the role of output (observation) signals for the Kalman filter based observer. Note that, in this work, all measurements are unfiltered (raw) signals.

4.1. *Ground Reaction Force*

The ground reaction force can be directly estimated using the FSR sensors. In the case of Nao robot, for instance, each foot possesses 4 FSR sensors with a force range between 0 and 25N, and the ground reaction force f_n^o is given by:

$$f_n^o = -\left(\underbrace{\sum_{i=1}^{4} \mathcal{F}_i^R}_{\text{right foot}} + \underbrace{\sum_{i=1}^{4} \mathcal{F}_i^L}_{\text{left foot}} \right) \tag{12}$$

where $\mathcal{F}_i^*$ is the force measured at the i^{th} FSR.

4.2. *ZMP*

Recall that the ZMP and Center of Pressure (CoP) coincide when the robot is in a stable configuration [19]. Thus, the ZMP can be computed as follows:

$$\begin{aligned} p_x = x_{CoP} &= \frac{\sum_{i=1}^{4} \mathcal{F}_i^R \, x_i^R + \sum_{i=1}^{4} \mathcal{F}_i^L \, x_i^L}{|f_n^o|} \\ p_y = y_{CoP} &= \frac{\sum_{i=1}^{4} \mathcal{F}_i^R \, y_i^R + \sum_{i=1}^{4} \mathcal{F}_i^L \, y_i^L}{|f_n^o|} \end{aligned} \tag{13}$$

where f_n^o is defined in (12), and x_i^* and y_i^* are the x and y positions of the i^{th} FSR in the foot frame.

4.3. *CoM Acceleration*

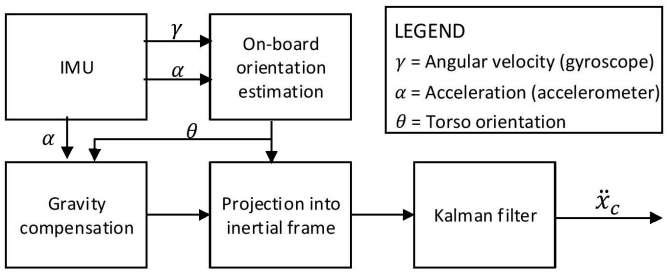

Fig. 4. Block diagram of the processing done on the raw acceleration data

The acceleration of the CoM can be directly extracted from the IMU, which is a standard part of a humanoid robot sensors. As for Nao, the IMU provides measurements from a three-axis accelerometer and a two-axis gyroscope. We assume

that the CoM coincides with the IMU. Therefore, the accelerometer data can be used to approximate the acceleration of the CoM.

Fig. 4 presents a block diagram of the raw acceleration data processing. The projection into an inertial frame and the gravity compensation steps are implemented as presented in [20].

4.4. *CoM Position*

The CoM position in the support foot frame can be easily obtained by a simple forward kinematics.

5. External Force Observer

The first component of the external force applied to the humanoid robot that can be directly estimated from the FSR information is F_z using (5). Then the horizontal components F_x and F_y can be estimated using (7).

5.1. *Estimating F_z*

To estimate F_z, Eq. (5) is discretized with a sampling time T to obtain the following linear dynamic system:

$$\begin{aligned} \boldsymbol{\mathcal{Z}}(k+1) &= \boldsymbol{A}\,\boldsymbol{\mathcal{Z}}(k) + \boldsymbol{B}\,\boldsymbol{u}_z(k) \\ \boldsymbol{Y}_z(k) &= \boldsymbol{C}_z\,\boldsymbol{\mathcal{Z}}(k) + \boldsymbol{v}_z(k) \end{aligned} \tag{14}$$

where:

- The state vector $\boldsymbol{\mathcal{Z}}$ is given by:
$$\boldsymbol{\mathcal{Z}}(k) = \begin{bmatrix} z_c(kT) & \dot{z}_c(kT) & \ddot{z}_c(kT) & F_z(kT) & \dot{F}_z(kT) \end{bmatrix}^T$$
- The input signal $\boldsymbol{u}_z$ in given by:
$$\boldsymbol{u}_z(k) = \begin{bmatrix} \dddot{z}_c(kT) & \ddot{F}_z(kT) \end{bmatrix}^T$$
where $\dddot{z}_c(kT)$ is the acceleration derivative, which is usually called the jerk.
- The output signal $\boldsymbol{Y}_z$ is given by:
$$\boldsymbol{Y}_z(k) = \begin{bmatrix} z_c(kT) & \ddot{z}_c(kT) & f_n^o(kT) + M_c\,g \end{bmatrix}^T$$
- The model constant matrices $\boldsymbol{A}$, $\boldsymbol{B}$ and $\boldsymbol{C}_z$ are given by:
$$\boldsymbol{A} = \begin{bmatrix} 1 & T & \frac{T^2}{2} & 0 & 0 \\ 0 & 1 & T & 0 & 0 \\ 0 & 0 & 1 & 0 & 0 \\ 0 & 0 & 0 & 1 & T \\ 0 & 0 & 0 & 0 & 1 \end{bmatrix}, \quad \boldsymbol{B} = \begin{bmatrix} \frac{T^3}{6} & 0 \\ \frac{T^2}{2} & 0 \\ T & 0 \\ 0 & \frac{T^2}{2} \\ 0 & T \end{bmatrix}$$
$$\boldsymbol{C}_z = \begin{bmatrix} 1 & 0 & 0 & 0 & 0 \\ 0 & 0 & 1 & 0 & 0 \\ 0 & 0 & -M_c & 1 & 0 \end{bmatrix}$$

(15)

- $\boldsymbol{v}_z$ is the observation noise and considered as a Gaussian white noise with a covariance matrix $\boldsymbol{R}_z$. Thus, $\boldsymbol{v}_z \sim N(\boldsymbol{0}, \boldsymbol{R}_z)$.

To formulate the estimation problem as a Kalman filter, we reformulate the dynamic system in (14) as follows:

$$\begin{aligned} \boldsymbol{\mathcal{Z}}(k+1) &= \boldsymbol{A}\,\boldsymbol{\mathcal{Z}}(k) + \boldsymbol{\omega}_z(k) \\ \boldsymbol{Y}_z(k) &= \boldsymbol{C}_z\,\boldsymbol{\mathcal{Z}}(k) + \boldsymbol{v}_z(k) \end{aligned} \tag{16}$$

where $\boldsymbol{\omega}_z(k) = \boldsymbol{B}\,\boldsymbol{u}_z(k)$ becomes the process noise. $\boldsymbol{\omega}_z$ is supposed to be a Gaussian white noise with a covariance $\boldsymbol{Q}$, i.e. $\boldsymbol{\omega}_z \sim N(\boldsymbol{0}, \boldsymbol{Q})$, independent of $\boldsymbol{v_z}$. The matrix $\boldsymbol{Q}$ is given by:

$$\boldsymbol{Q} = \boldsymbol{B} \begin{bmatrix} \sigma^2_{\dddot{z}_c} & 0 \\ 0 & \sigma^2_{\ddot{F}_z} \end{bmatrix} \boldsymbol{B}^T \tag{17}$$

where $\sigma^2_{\dddot{z}_c}$ and $\sigma^2_{\ddot{F}_z}$ are respectively the covariance of $\dddot{z}_c$ and $\ddot{F}_z$.

By applying Kalman filter on (16), an estimation of the state vector is obtained:

$$\hat{\boldsymbol{\mathcal{Z}}}(k) = \begin{bmatrix} \hat{z}_c(kT) & \hat{\dot{z}}_c(kT) & \hat{\ddot{z}}_c(kT) & \hat{F}_z(kT) & \hat{\dot{F}}_z(kT) \end{bmatrix}^T \tag{18}$$

5.2. *Estimating F_x and F_y*

As above-mentioned F_x and F_y can be estimated from (7). However, because of the similarity between the two components of ZMP (p_x and p_y), we only consider the estimation of F_x as F_y can be estimated in an analogous way.

At first, p_x in (7) is discretized with a sampling time T to obtain the following linear dynamic system:

$$\begin{aligned} \boldsymbol{\mathcal{X}}(k+1) &= \boldsymbol{A}\,\boldsymbol{\mathcal{X}}(k) + \boldsymbol{\omega}_x(k) \\ \boldsymbol{Y}_x(k) &= \boldsymbol{C}_x\,\boldsymbol{\mathcal{X}}(k) + \boldsymbol{v}_x(k) \end{aligned} \tag{19}$$

where:

- $\boldsymbol{\mathcal{X}}(k)$, $\boldsymbol{\omega}_x(k)$, $\boldsymbol{v}_x$, $\boldsymbol{A}$ and $\boldsymbol{Q}$ are defined in the same way as in Section 5.1 by replacing F_z by F_x and z_c by x_c.
- The output signal $\boldsymbol{Y}_x$ is given by:

$$\boldsymbol{Y}_x(k) = \begin{bmatrix} x_c(kT) & \ddot{x}_c(kT) & p_x(kT) \end{bmatrix}^T$$

- The output matrix $\boldsymbol{C}_x$ is given by:

$$\boldsymbol{C}_x = \begin{bmatrix} 1 & 0 & 0 & 0 & 0 \\ 0 & 0 & 1 & 0 & 0 \\ 1 & 0 & \frac{M_c\,\hat{z}_c(kT)}{\hat{f}^o_n(kT)} & -\frac{\hat{z}_c(kT)}{\hat{f}^o_n(kT)} & 0 \end{bmatrix}$$

$\hat{z}_c(kT)$ and $\hat{f}_n^o(kT) = -M_c\, g - M_c\, \hat{\ddot{z}}_c(kT) + \hat{F}_z(kT)$ are computed using (18).

By applying Kalman filter on (19), an estimation of the state vector $\boldsymbol{\mathcal{X}}$ is obtained:

$$\hat{\boldsymbol{\mathcal{X}}}(k) = \begin{bmatrix} \hat{x}_c(kT) & \hat{\dot{x}}_c(kT) & \hat{\ddot{x}}_c(kT) & \hat{F}_x(kT) & \hat{\dot{F}}_x(kT) \end{bmatrix}^T \tag{20}$$

The observer implementation architecture is summarized in Fig. 5.

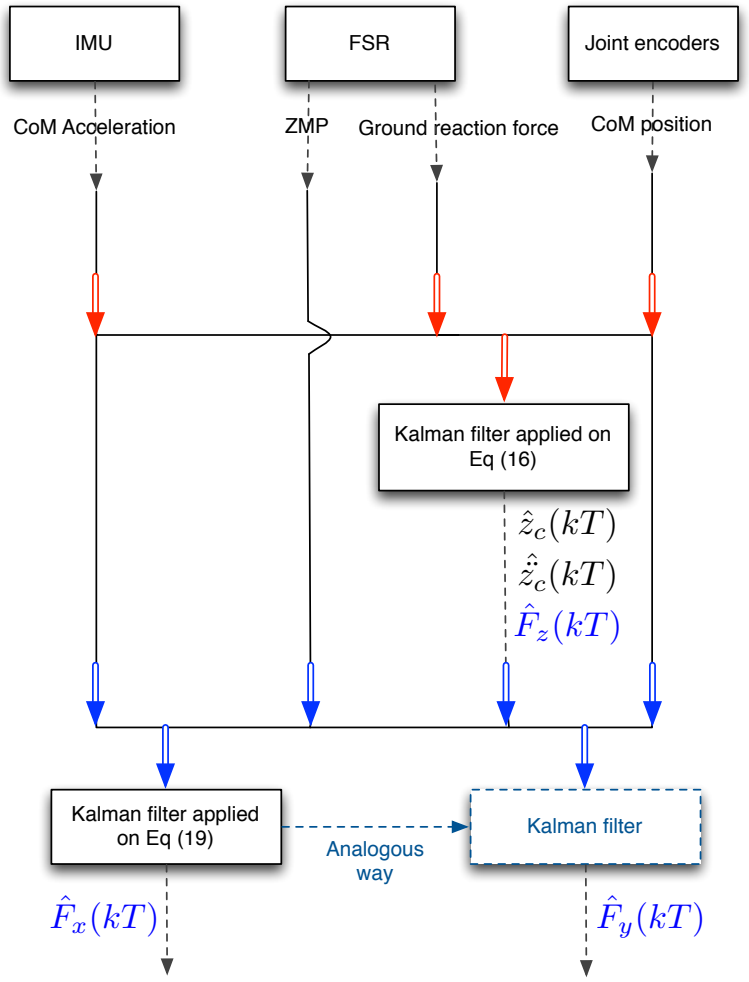

Fig. 5. Block diagram of the external force observer $\hat{\boldsymbol{F}}^{ext} = [\hat{F}_x\ \hat{F}_y\ \hat{F}_z]^T$

6. Experimental Results

The observer has been experimentally validated on the Nao robot through four scenarios, and it has also been used to accomplish human-robot interaction tasks.

For the reported experiments results, the following parameters were used: $g = 9.81\ m.s^{-2}$, $T = 16.7$ ms ($F = 60$ Hz) and $M_c = 5.19$ kg.

Regarding the observer parameters, for the **experiments 1, 2 and 3**, the best results have been obtained with:

$$\begin{aligned} &\sigma^2_{\dddot{x}} = \sigma^2_{\dddot{y}} = \sigma^2_{\dddot{z}} = 10^3 \\ &\sigma^2_{\ddot{F}_x} = \sigma^2_{\ddot{F}_y} = \sigma^2_{\ddot{F}_z} = 10^3 \\ &\boldsymbol{R}_z = \begin{bmatrix} 0.01 & 0 & 0 \\ 0 & 1 & 0 \\ 0 & 0 & 1 \end{bmatrix}, \boldsymbol{R}_x = \boldsymbol{R}_y = \begin{bmatrix} 0.01 & 0 & 0 \\ 0 & 1 & 0 \\ 0 & 0 & 0.01 \end{bmatrix} \end{aligned} \tag{21}$$

While for the **experiment 4**, the following parameters have been used:

$$\begin{aligned} &\sigma^2_{\dddot{x}} = \sigma^2_{\dddot{y}} = \sigma^2_{\dddot{z}} = 10^2 \\ &\sigma^2_{\ddot{F}_x} = \sigma^2_{\ddot{F}_y} = \sigma^2_{\ddot{F}_z} = 10^3 \\ &\boldsymbol{R}_z = \begin{bmatrix} 0.1 & 0 & 0 \\ 0 & 1 & 0 \\ 0 & 0 & 1 \end{bmatrix}, \boldsymbol{R}_x = \boldsymbol{R}_y = \begin{bmatrix} 0.1 & 0 & 0 \\ 0 & 1 & 0 \\ 0 & 0 & 0.1 \end{bmatrix} \end{aligned} \tag{22}$$

As we mentioned before, the experimental data as well as C++/ROS implementation and the MATLAB code that has been used to produce the results in this paper can be downloaded here[c]. These data and code could be helpful to the humanoid robotics community with the objective of benchmarking or comparing with other approaches.

6.1. *Force Applied to the Robot Torso*

In this experiment, a force in the $x-z$ plane is applied through a spring-based force meter as shown in Fig. 6(a). Since the torso frame is close to the CoM position of the robot, the magnitude of resulting moment applied to the LIP model is relatively small. Therefore, applying a force to the robot torso is practically equivalent to applying it to its CoM.

The F_x and F_y components of the force can be easily obtained by the following formula:

$$\begin{aligned} F_x &= \|F^{ext}\| \cos(\theta) \\ F_z &= \|F^{ext}\| \sin(\theta) \end{aligned} \tag{23}$$

where $\|F^{ext}\|$ is the force magnitude measured with the force meter, and θ is the angle between the force meter and the x axis, the positive direction of rotation is defined to be clockwise.

[c]https://goo.gl/VkhejY

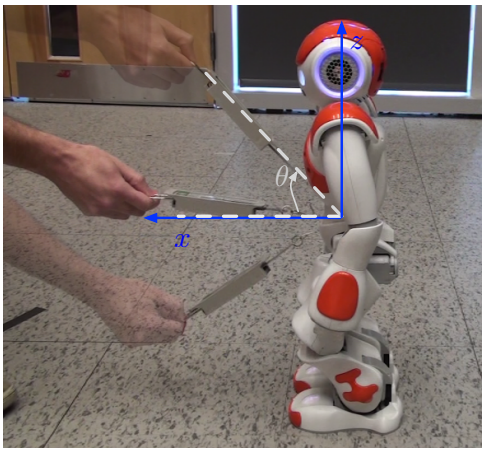

(a) Experimental setup

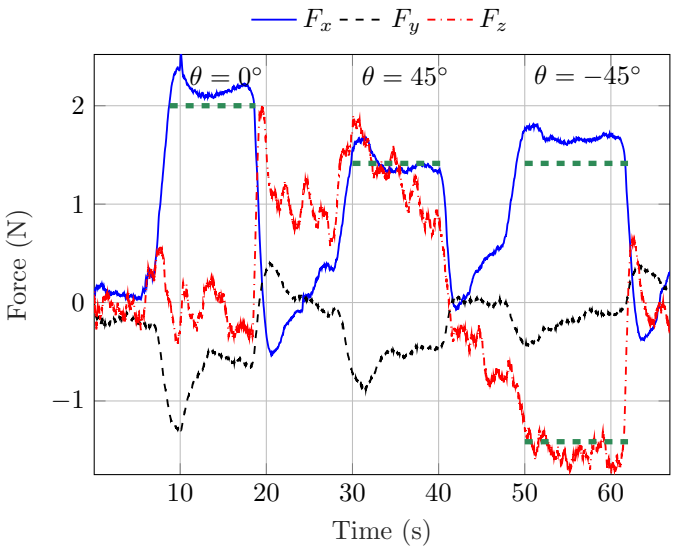

(b) Estimating the three components of F^{ext}. The expected force is in green dashed line.

Fig. 6. **Experiment 1**: Applying a fixed-magnitude force in the $x - z$ plane.

The experiment consists of applying a force with a constant magnitude of approximately 2N in the $x - z$ plane but with different values of the angle θ.

Fig. 6(b) shows the overall performance of the observer, it points out that the observer reasonably succeeds in estimating the three components of the external force. However, note that the main difficulty in this experiment was keeping a force with constant magnitude by only visually monitoring the force indicator. Moreover, the angle (θ) was also visually monitored using a protractor.

We can also notice that the observer detects non-zero force along y axis, this is mainly due to the difficulty of keeping the force meter in the vertical plane.

6.2. *Applying a Force to a Point of the Robot Arm*

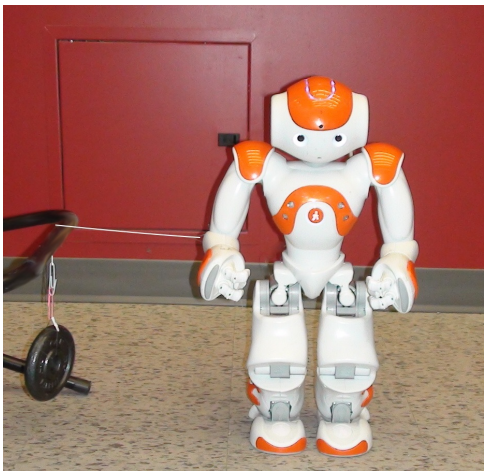

(a) Experimental setup

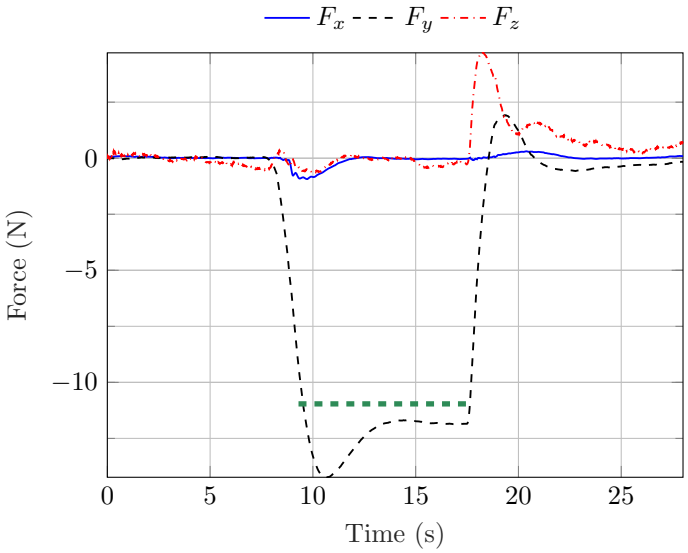

(b) Estimating the three components of F^{ext}. The expected force is in green dashed line.

Fig. 7. **Experiment 2**: Applying a force along y axis

(a) Experimental setup

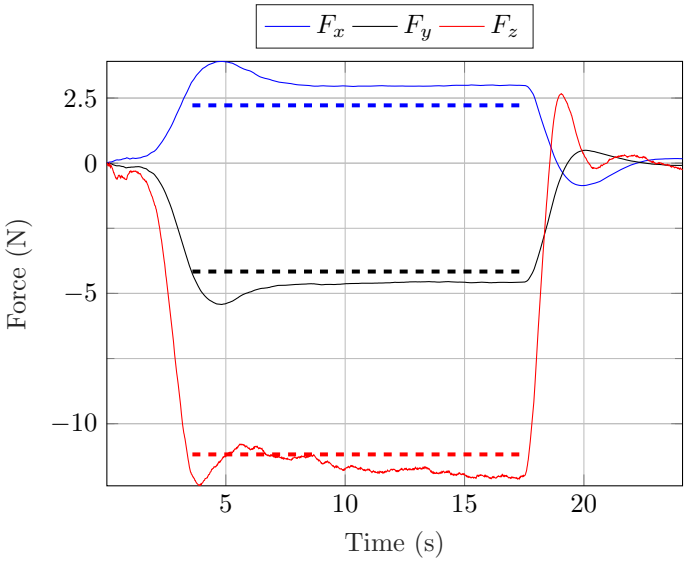

(b) Estimating the three components of F^{ext} and its norm, the expected forces are in dashed lines

Fig. 8. **Experiment 3**: Applying an arbitrary external force

The setup for the second and third scenarios are respectively presented in Fig. 7(a) and Fig. 8(a), and the attached mass $m_o = 2.5$ pounds (1.13 kg). In both experiments, a force of around 11 N has been applied to the robot right arm, first along the y axis in Fig. 7(a) and then along the z axis in Fig. 8(a).

By applying inverse dynamics to the kinematic chain from the point at which the force is applied to the robot's CoM, the wrench vectors in the second and third experiments as well as the virtual forces, as defined in (11), are respectively:

$$\begin{aligned}
\boldsymbol{\mathcal{W}}_2 = \begin{bmatrix} \boldsymbol{F}_2^{ext} \\ \boldsymbol{\tau}_2^{ext} \end{bmatrix} \approx \begin{bmatrix} 0.0 \\ -11.12 \\ 0.0 \\ -0.05 \\ 0.0 \\ -0.08 \end{bmatrix} \Longrightarrow \hat{\boldsymbol{F}}_2^{ext} \approx \begin{bmatrix} 0.0 \\ -10.96 \\ 0 \end{bmatrix} \\
\boldsymbol{\mathcal{W}}_3 = \begin{bmatrix} \boldsymbol{F}_3^{ext} \\ \boldsymbol{\tau}_3^{ext} \end{bmatrix} \approx \begin{bmatrix} 0.0 \\ 0.0 \\ -11.12 \\ 1.31 \\ 0.70 \\ 0.0 \end{bmatrix} \Longrightarrow \hat{\boldsymbol{F}}_3^{ext} \approx \begin{bmatrix} 2.22 \\ -4.16 \\ -11.12 \end{bmatrix}
\end{aligned} \tag{24}$$

Those three experiments are very similar to the experiments conducted in [14]. As such, they can be used as a benchmark to compare with their results. Fig. 7(b) and Fig. 8(b) show that the proposed observer succeeds in estimating the corresponding virtual external force since the estimated force is reasonably close to the expected one.

The authors in [14] point out that the estimated force, by their method, has an important magnitude instead of a small one when the mass is removed. They argue that their main sources of error are the unmodeled static friction and the low-cost hardware of Nao robot, for instance, plastic joint gears. On the other hand, the estimated force by our observer after removing the mass has a small magnitude of around 0.5 N, which is an order of magnitude smaller than the results in [14]. Furthermore, those results also show the robustness of our observer to the sources of error identified in [14].

6.3. *Walking with an External Force*

The experimental setup used in this case study is given in Fig. 9(a). Initially, the robot is standing still and attached from the waist to a mass which is in full contact with the ground. The robot then starts walking forward. At some point, the cable (fishing line) becomes completely tensed and the mass is lifted off the ground by the walking robot, as shown in Fig. 9(b). The lifted mass ($m_0 \approx 300$ g) generates a force of approximately 3N, which acts as an external force pulling the robot backwards. Note that when the rope is tensed, a small angle $\alpha \approx 5^\circ$ is formed between the cable and the x axis.

The experimental results of a forward walk with an external force are presented in Fig. 10. The estimated F_x and F_y components of the external force F_{ext} are given in Fig. 10(a), while the F_z component is given in Fig. 10(b). Fig. 10 shows that the

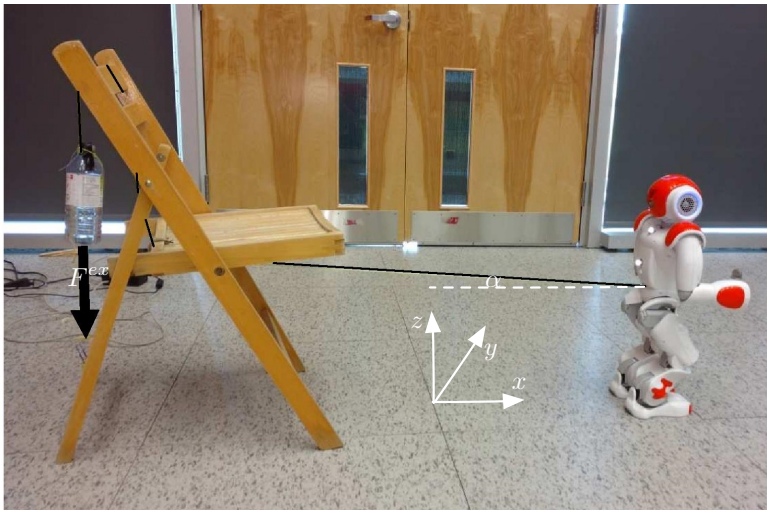

(a) Experimental setup

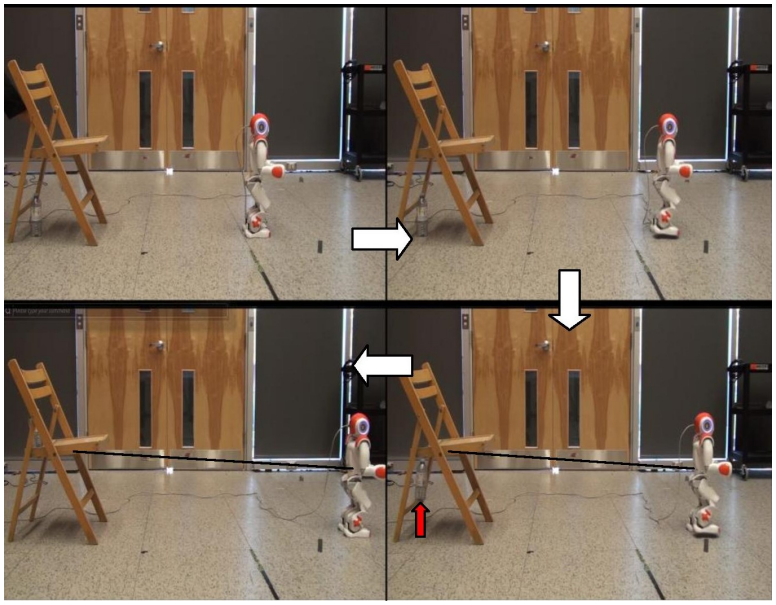

(b) Snapshots of an experiment where a mass is lifted off the floor by a Nao robot walking forward

Fig. 9. **Experiment 4**: Applying an external force to a walking robot. The cable has been coloured in black for clarity

observer can estimate the components F_x and F_y within a reasonable margin of error while the F_z component is more challenging in the case of a walking robot. Moreover, the robot has been pulled backward around the time $t = 4\,s$. This was

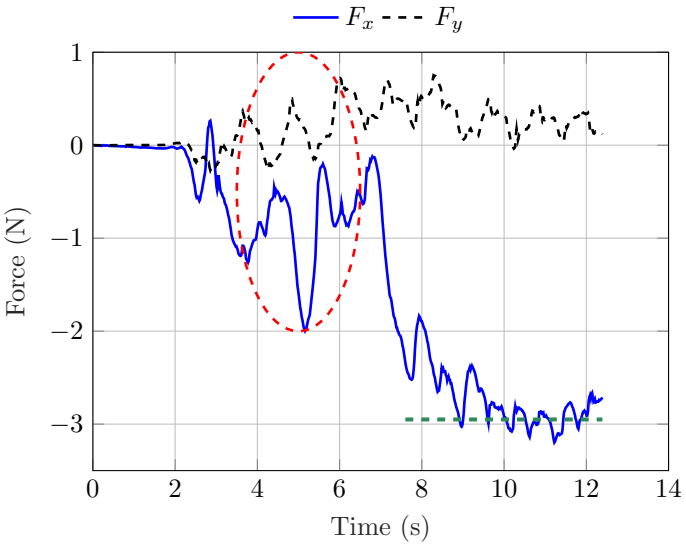

(a) Estimating F_x and F_y

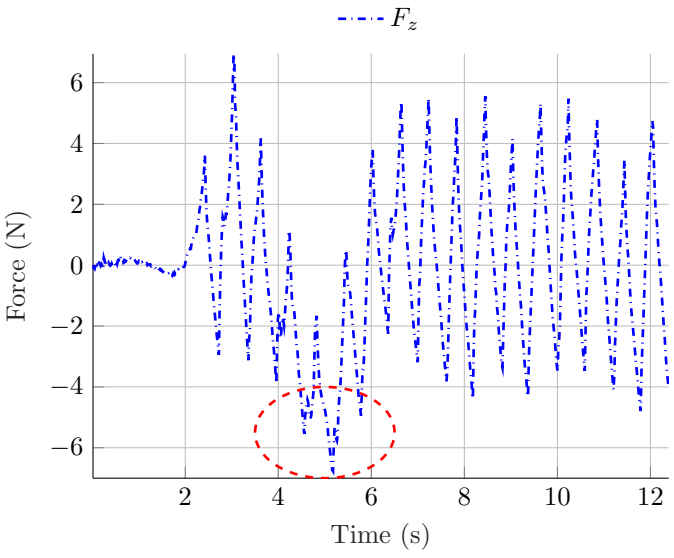

(b) Estimating F_z

Fig. 10. **Experiment 4**: Estimating the components of the external force $F^{ext} = [F_x\, F_y\, F_z]^T$, the expected force is in green dashed line.

caused by the elasticity of the cable and its friction with the experimental structure, which explains the results of the observer in the dashed-red encircled area in Fig. 10.

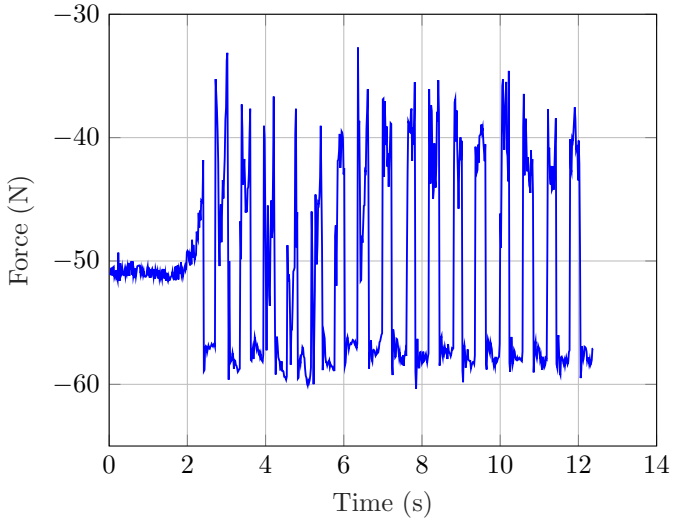

Fig. 11. **Experiment 4**: The total normal force (f_n^o) applied to the robot feet

Analyzing the estimated F_x points out that the observer correctly estimated the pulling force that propagated to the robot through the cable. However, some oscillations can be observed, which are caused by the cable elasticity on one hand, and because of the mass acceleration on the other. In fact the external force is $F_x = -m_0 (g + \ddot{z}_0) \approx -m_0 (g + \ddot{x}_c)$, where $\ddot{z}_0$ is the object acceleration along z axis.

By analyzing the total normal force applied to the robot feet, we can observe that the force is varying roughly between -35 and -60 N. A deeper analysis revealed that some of the FSR have lost contact with the ground during the walking experiment. As a result, the observer estimated that an external force along the z axis (F_z) were applied.

6.4. *Compliant Arm Control*

As an application of our observer, we implemented a compliant controller of the robot arms as a function of the detected force. A snapshot of the experiment is given in Fig. 12.

However, during the experiment we observed that the observer performance degraded. The main problem is that the interaction between the robot and the human often caused a bad contact between the feet and the floor, which results in unreliable data from the FSR.

Thereby, to implement a compliance control of Nao arms, we combined the proposed force observer with a joint level compliance strategy. It is well known that it is possible to estimate the magnitude and direction of an external force applied to a manipulator if an accurate dynamic model of the robot is available and if

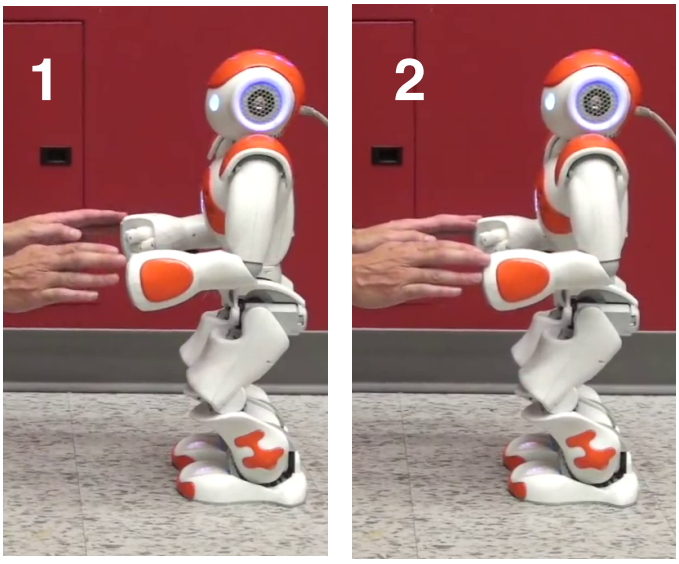

Fig. 12. Compliant control of the robot arms

the torques applied by the motors are known [21, 22]. This approach can also be extended to humanoid robots [14], albeit it is more difficult since humanoid robots are floating-base robots.

First, the torque due to the robot dynamics must be isolated. To do so, it is possible to use the following inverse dynamic equation:

$$\begin{aligned} \boldsymbol{\tau}_m &= \boldsymbol{B}(\boldsymbol{q})\,\ddot{\boldsymbol{q}} + \boldsymbol{C}(\boldsymbol{q},\dot{\boldsymbol{q}})\,\dot{\boldsymbol{q}} + \boldsymbol{g}(\boldsymbol{q}) + \boldsymbol{J}^T(\boldsymbol{q})\,\boldsymbol{F}^{ext} \\ &\triangleq \hat{\boldsymbol{\tau}} + \boldsymbol{J}^T(\boldsymbol{q})\,\boldsymbol{F}^{ext} \end{aligned} \tag{25}$$

where J is the Jacobian matrix of the considered chain, τ_m is the measured joint torques, $B(q)$ is the inertia matrix, $C(q,\dot{q})\,\dot{q}$ includes the Coriolis and centrifugal forces, $g(q)$ is the gravity term, F^{ext} is the external force applied at the end-effector, and $q, \dot{q}, \ddot{q}$ are respectively the position, velocity and acceleration of the joints.

The external force can then be easily obtained by subtracting this torque from the measured one to get the external force applied to the humanoid arms:

$$\boldsymbol{F}^{ext} = \boldsymbol{J}^{\dagger T}(\boldsymbol{q})\,(\boldsymbol{\tau}_m - \hat{\boldsymbol{\tau}}) \tag{26}$$

where $J^\dagger$ is the pseudo-inverse of matrix J.

Referring to Nao robots official documentation [23], the Nao motors are controlled through a PD controller, making it possible to determine the motor output torque with the following linear approximation:

$$\tau_m^i = K_m\,(q_d - q_e) \tag{27}$$

where τ_m^i is the torque for the motor i, $(q_d - q_e)$ is the position error and K_m is

a constant coefficient that depends on multiple parameters of the joint motor (e.g. reduction ratio). The block diagram of the modified observer is given in Fig. 13.

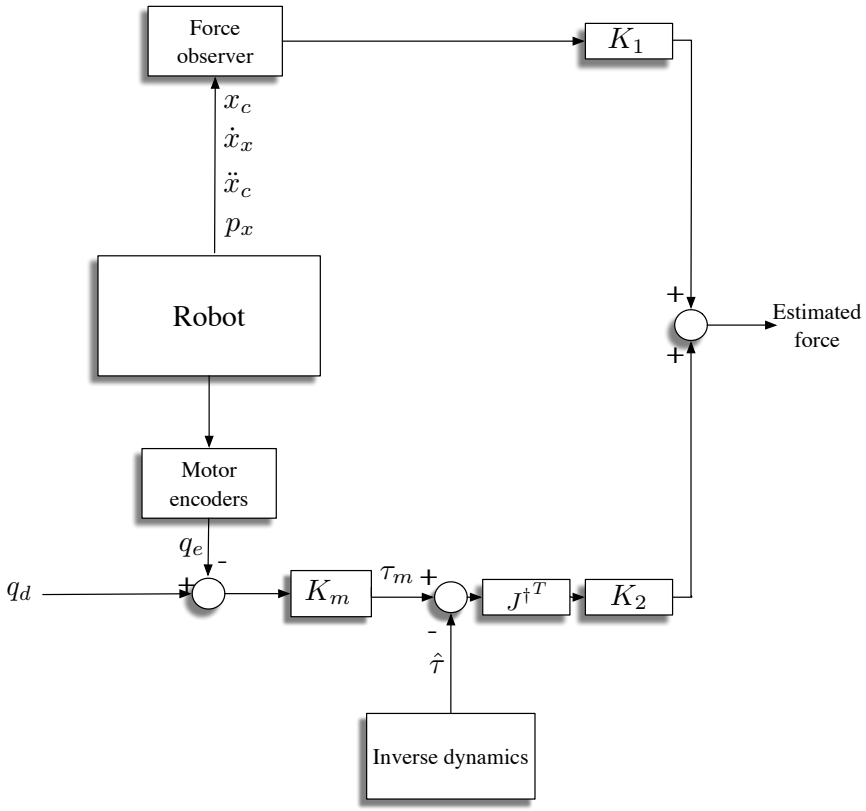

Fig. 13. Arm Compliance Controller

K_1 and K_2 are proportional gains, they can be chosen as constant parameters such as $K_1 + K_2 = 1$, or dynamically as follows:

$$\begin{aligned} K_1 &= \frac{K_a}{K_t} \\ K_2 &= 1 - K_1 \end{aligned} \tag{28}$$

where K_a is the number of active FSR that are in contact with the ground, and K_t is the total number of FSR, which is in the case of Nao robot equal to 8. It can be noticed that with this strategy, the observer based on inverse dynamics only reacts when at least one FSR loses contact with the ground.

The performance of the compliance controller was validated by a spring-based force sensor. By applying the proposed observer to estimate the force along the x

axis (F_x), we implemented the arm compliance as follows:

$$x_h = x_h^0 + \frac{1}{k} F_x \tag{29}$$

where x_h and x_h^0 are respectively the desired position of the hand and its initial position along the x axis, k is a virtual spring constant and F_x is the detected force along x axis. We chose a stiffness coefficient $k = 50\, Nm^{-1}$.

Fig. 14 shows the performance of the proposed observer and the compliance controller.

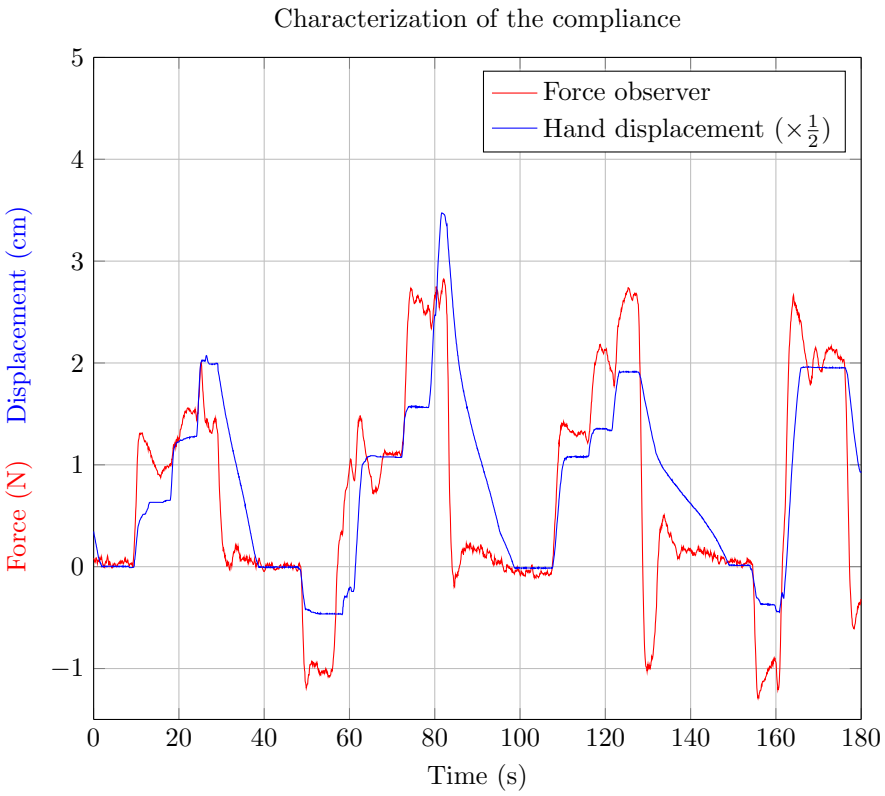

Fig. 14. Displacement of the arms and the estimated external force using the observer in Fig. 13

6.5. *Compliant Human-Robot Interaction*

As a second application, we have implemented an interactive walking based on the interaction between the robot and a human as shown in Fig. 15. In this scenario, the robot walks in the direction of the detected force (forward or backward) if the force

magnitude exceeds a predefined threshold, and stops if the magnitude of detected force is less than the threshold.

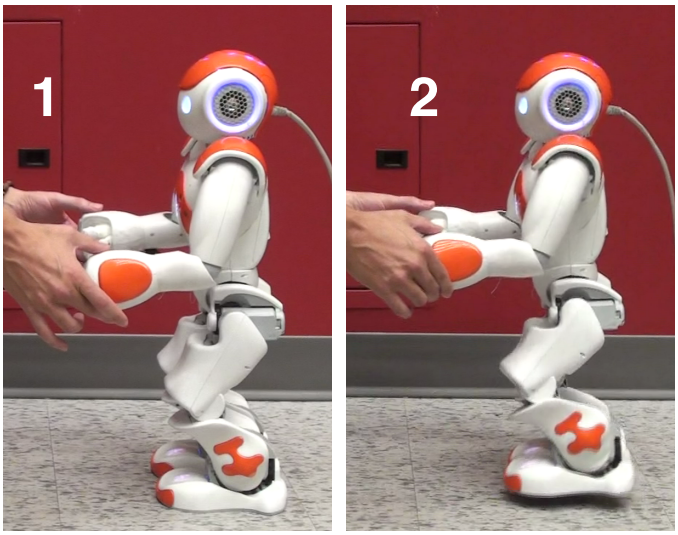

Fig. 15. Interactive walking by applying a sagittal guidance force to the robot hands

7. Conclusion

In this paper, we introduced a Kalman filter based observer to estimate the three components of an external force applied to a small or medium-sized humanoid robot. In contrast to conventional methods that are mainly based on the use of expensive 6-axis force/torque sensors, the proposed observer uses measurement from force-sensing resistors (FSR) located under the feet of the robot and the information from the robot's IMU sensor. This observer was extensively tested on a Nao robot and the results revealed that it overcomes the limitations of the related approaches in the literature, which are mainly caused by the low-cost hardware components of the robot.

However, there is still room for improvement, for instance, the covariance matrices R and Q in the observer implementation have been experimentally identified, however, they can be estimated using some existing methods in the literature, such as [24]. Moreover, even though the objective of our observer is to estimate an equivalent force, called virtual force, that is applied to the CoM frame, it is possible to combine it with methods for identifying the contact point, such as [25]. This would allow the observer to provide the external force components at the contact point and in the world frame by a simple inverse dynamics calculation.

Furthermore, our experiments revealed that the performance of the observer can degrade when one or more of the FSR lose contact with the ground. One of the

reasons of this phenomenon is the rigid design of the foot sole. A possible solution could be to replace the rigid sole by a soft and compliant one and to embed the FSR inside the flexible sole.

Future work will focus on integrating the external force observer into the pattern generator module, and human-humanoid robot or multiple humanoid robots collaborative tasks.

Acknowledgment

This research is supported by the Natural Sciences and Engineering Research Council of Canada (NSERC).

References

1. Louis Hawley, Rémy Rahem, and Wael Suleiman. Kalman filter based observer for an external force applied to medium-sized humanoid robots. In *IEEE International Conference on Intelligent Robots and Systems*, pages 1204–1211, 2018.
2. Antoine Rioux and Wael Suleiman. Humanoid navigation and heavy load transportation in a cluttered environment. In *IEEE/RSJ International Conference on Intelligent Robots and Systems (IROS)*, pages 2180–2186, 2015.
3. Antoine Rioux and Wael Suleiman. Autonomous SLAM based humanoid navigation in a cluttered environment while transporting a heavy load. *Robotics and Autonomous Systems*, 99:50–62, 2018.
4. Antoine Rioux, Claudia Esteves, Jean-Bernard Hayet, and Wael Suleiman. Cooperative Vision-Based Object Transportation by Two Humanoid Robots in a Cluttered Environment. *International Journal of Humanoid Robotics*, 14(03):1–30, 2017.
5. Louis Hawley and Wael Suleiman. Control framework for cooperative object transportation by two humanoid robots. *Robotics and Autonomous Systems*, 115:1 – 16, 2019.
6. Erhan Oztop, David W. Franklin, Thierry Chaminade, and Gordon Cheng. Human–humanoid interaction: Is a humanoid robot perceived as a human? *International Journal of Humanoid Robotics*, 02(04):537–559, 2005.
7. Kensuke Harada, Shuuji Kajita, Kenji Kaneko, and Hirohisa Hirukawa. ZMP Analysis for Arm / Leg Coordination. In *IEEE/RSJ International Conference on Intelligent Robots and Systems*, pages 75–81, 2003.
8. Kensuke Harada, Shuuji Kajita, Kenji Kaneko, and Hirohisa Hirukawa. Pushing manipulation by humanoid considering two-kinds of ZMPs. *IEEE International Conference on Robotics and Automation*, pages 1627–1632, 2003.
9. Kensuke Harada, Shuuji Kajita, Hajime Saito, Mitsuharu Morisawa, Fumio Kanehiro, Kiyoshi Fujiwara, Kenji Kaneko, and Hirohisa Hirukawa. A humanoid robot carrying a heavy object. In *IEEE International Conference on Robotics and Automation (ICRA)*, pages 1712–1717, 2005.
10. Kenji Kaneko, Fumio Kanehiro, Mitsuharu Morisawa, Eiichi Yoshida, and Jean-Paul Laumond. Disturbance observer that estimates external force acting on humanoid robots. *12th IEEE International Workshop on Advanced Motion Control (AMC)*, pages 1–6, 2012.
11. Mehdi Benallegue, Pierre Gergondet, Hervé Audren, Alexis Mifsud, Mitsuharu Morisawa, Florent Lamiraux, Abderrahmane Kheddar, and Fumio Kanehiro. Model-based external force/moment estimation for humanoid robots with no torque measurement.

In *IEEE International Conference on Robotics and Automation (ICRA)*, pages 3122 – 3129, 2018.
12. Kenji Kaneko, Fumio Kanehiro, Shuuji Kajita, Mitsuharu Morisawa, Kiyoshi Fujiwara, Kensuke Harada, and Hirohisa Hirukawa. Slip observer for walking on a low friction floor. In *IEEE/RSJ International Conference on Intelligent Robots and Systems (IROS)*, pages 1457–1463, 2005.
13. David Gouaillier, Vincent Hugel, Pierre Blazevic, Chris Kilner, Jerome Monceaux, Pascal Lafourcade, Brice Marnier, Julien Serre, and Bruno Maisonnier. Mechatronic design of NAO humanoid. *IEEE International Conference on Robotics and Automation*, pages 769–774, 2009.
14. Tommaso Mattioli and Marilena Vendittelli. Interaction Force Reconstruction for Humanoid Robots. *IEEE Robotics and Automation Letters*, 2(1):282–289, 2017.
15. Nicholas Rotella, Alexander Herzog, Stefan Schaal, and Ludovic Righetti. Humanoid Momentum Estimation Using Sensed Contact Wrenches. In *IEEE-RAS International Conference on Humanoid Robots*, pages 556–563, 2015.
16. Louis Hawley and Wael Suleiman. External Force Observer for Medium-sized Humanoid Robots. In *IEEE-RAS International Conference on Humanoid Robots*, pages 366–371, 2016.
17. Erik Berger, David Vogt, Nooshin Haji-Ghassemi, Bernhard Jung, and Heni Ben Amor. Inferring guidance information in cooperative human-robot tasks. In *IEEE-RAS International Conference on Humanoid Robots*, pages 124–129, 2015.
18. Justin Carpentier, Mehdi Benallegue, and Nicolas Mansard. Center-of-Mass Estimation for a Polyarticulated System in Contact — A Spectral Approach. *IEEE Transactions on Robotics*, 32(4):810–822, 2016.
19. Miomir Vukobratović and Branislav Borovac. Zero-Moment Point — Thirty Five Years of Its Life. *International Journal of Humanoid Robotics*, 01(01):157–173, 2004.
20. Marco Bellaccini, Leonardo Lanari, Antonio Paolillo, and Marilena Vendittelli. Manual guidance of humanoid robots without force sensors: Preliminary experiments with NAO. *IEEE International Conference on Robotics and Automation*, pages 1184–1189, 2014.
21. Emanuele Magrini, Fabrizio Flacco, and Alessandro De Luca. Estimation of contact forces using a virtual force sensor. In *IEEE International Conference on Intelligent Robots and Systems (IROS)*, pages 2126–2133, 2014.
22. Emanuele Magrini, Fabrizio Flacco, and Alessandro De Luca. Control of generalized contact motion and force in physical human-robot interaction. In *IEEE International Conference on Robotics and Automation (ICRA)*, pages 2298–2304, 2015.
23. Aldebaran. Nao official documentation, 2016.
24. R. Mehra. On the identification of variances and adaptive kalman filtering. *IEEE Transactions on Automatic Control*, 15(2):175–184, April 1970.
25. Fabrizio Flacco and Abderrahmane Kheddar. Contact detection and physical interaction for low cost personal robots. In *IEEE International Symposium on Robot and Human Interactive Communication (RO-MAN)*, 2017.